


Article

Parametric Study of Structured UTM Separation Recommendations with Physics-Based Monte Carlo Distribution for Collision Risk Model

Chung-Hung John Wang ¹, Chao Deng ¹ and Kin Huat Low ^{2,*}¹ Air Traffic Management Research Institute, Nanyang Technological University, Singapore 639798, Singapore² The School of Mechanical and Aerospace Engineering, Nanyang Technological University, Singapore 639798, Singapore

* Correspondence: mkhlow@ntu.edu.sg

Abstract: With the increasing demand for unmanned aircraft system (UAS) traffic management (UTM) airspace comes the need to ensure the safe operation and management of said airspace. One layer of defense against mid-air-collision and the ensuing third-party injury or fatality is the pre-flight separation assurance. This could be achieved by establishing the separation requirements for the UTM traffic based on the flight dynamics and communication navigation surveillance (CNS) performance that could be achieved in the airspace in question. A modified Reich collision risk model, typically used in civil aviation for separation minima evaluation, was used for the evaluation of the initial separation that would meet the target level of safety within a prescribed look-ahead time. This paper presents the parametric evaluation of using this physics-based and Monte Carlo-driven Reich collision risk model to evaluate the separation recommendation needed to achieve 10^{-7} mid-air-collision risk in UTM. The evaluation was conducted for an encounter pair consisting of identical ~ 1.2 kg quadrotors with various encounter geometries, cruise velocities, navigation uncertainties, and communication latency.

Keywords: UTM; separation; collision risk

Citation: Wang, C.-H.J.; Deng, C.; Low, K.H. Parametric Study of Structured UTM Separation Recommendations with Physics-Based Monte Carlo Distribution for Collision Risk Model. *Drones* **2023**, *7*, 345. <https://doi.org/10.3390/drones7060345>

Academic Editor: Carlos Tavares Calafate

Received: 18 April 2023

Revised: 19 May 2023

Accepted: 20 May 2023

Published: 25 May 2023



Copyright: © 2023 by the authors. Licensee MDPI, Basel, Switzerland. This article is an open access article distributed under the terms and conditions of the Creative Commons Attribution (CC BY) license (<https://creativecommons.org/licenses/by/4.0/>).

1. Introduction

Recent times have seen a push to open up the very-low-level airspace for air delivery or advance air mobility (AAM), often envisioned to take place in urban airspace, where the customer base is located. Unlike civil aviation, where the majority of infrastructures and operations are located in more rural environments due to noise concerns and infrastructure requirements, the management of urban-focused unmanned aircraft system (UAS) traffic management (UTM) airspace must also consider the risk to the wider range of third-party ground populations that could be affected. The management of such risk is especially important for an emerging service, as changes in public perception could make or break the fledgling industry.

Managing the public perception of an emerging service is especially tricky, as the introduction of this new mode of transportation would inherently increase the overall risk experienced by society with everything else held equal [1–3]. Another consideration is the difference in risk tolerance between first parties, who directly benefit from the newly introduced service, and third-parties, who have no right to participation in the activity and no control over the risk involved [1,4]. The perception of an acceptable level of safety would also differ for cargo- and passenger-carrying vehicles and with the scale of fatality from the accident [1,5].

While there exists no consensus on what the acceptable/target level of safety would need to be for the public to accept the additional risk from the introduction of UTM services, AAM manufacturers have often held 10^{-9} fatal accident/flight hours from civil aviation as

the benchmark figure [6]. For a UTM system with small UAS, the safety threshold could be reduced to 10^{-4} using the FN curve [7] and assuming that the fatality per accident (N) is reduced from 200 to 10; a risk-acceptance modifier for third parties (e.g., pedestrians) could be set to $\beta = 0.01$ due to the lack of control and benefit. The resulting risk target would agree with the proposed threshold of 10^{-7} for ground risk and third-party fatality due to mid-air collision (TLOS, or the target level of safety, from individual risk sources is cumulative when determining the overall TLOS) by the U-Space Bubble Project [8].

All these highlight the need for robust risk management in order for UTM to be generally accepted, and even more so in urban areas, where the affected parties could be much larger. However, a major obstacle in risk management is the lack of consensus on the UTM concept of operations (ConOps) that would help frame the operation conditions. For example, an air-route-based UTM ConOps would only need to manage risks along the established paths, while a free-fly UTM ConOps would need to manage risks dynamically in time and space. In the case of non-passenger-carrying UAS operations beyond the visual line of sight range, some of the major contributors to the creation of falling UAS debris include flight deviation into obstacles, system failures that interfere with controlled flights, and mid-air collision.

The current study focuses on the management and mitigation of mid-air collision within the UTM system through the determination and enforcement of separation recommendations. With the current lack of control, communication, and navigation infrastructure to handle free flight, the structured UTM along defined air routes with predictable encounter geometries might be the better option for managing collision risk and the resulting consequences in the urban setting. Note that separation standards in civil aviation generally include both wake-hazard and radar-performance separation consideration; the current study only focuses on the latter.

This paper presents the parametric study on UTM separation recommendation using a modified Monte Carlo-driven Reich collision risk model. The analysis was conducted using the example of an identical ~ 1.2 kg class quadrotor performing waypoint-to-waypoint (straight line) operation. A literature review on the current development in collision risk modeling, including advancement in collision detection and resolution (CD&R) and detect and avoid (DAA) in UTM, is presented and discussed in Section 2. An outline of the formulation used to develop the collision risk model for the present analysis is presented in Section 3. This is followed by the results and discussion (Section 4) and conclusion section (Section 5).

2. Literature Review

The introduction of separation requirements in civil aviation started with the practice of keeping the radar returns of air traffic on the primary surveillance radar screen from overlapping with each other, thus preventing mid-air collision in those more crowded airspaces [9]. The need for distance- or time-based separation eventually arose, as the increased traffic density over the less-well-monitored airspace, such as the oceanic crossings, demanded it. One of the most influential collision risk models, the Reich collision risk model, was devised to evaluate the separation minima for the North Atlantic crossing [10,11]. Reich collision relies on traffic data to derive the probabilistic distribution of the trailing aircraft and estimate the unmitigated collision risk over the communication time gap during the crossing. It has become the primary method for separation evaluation for strategic separation assurance for traffic and air-route planning in the International Civil Aviation Organization (ICAO) [12,13].

While strategic separation assurance should prevent the majority of loss-of-separation situations, tactical intervention by the controller and pilot is still needed in actual operations. For collision detection and resolution on a shorter time scale, a probabilistic or maximum range path prediction based on aircraft flight envelop might be used [14,15]; the former would be needed to determine risk-based resolution action, while the latter could be used as a boundary for conflict prevention against non-cooperative air traffic. On the

other hand, the airborne collision avoidance system version II (ACAS II) algorithm took a deterministic approach with the closest point of approach (CPA) calculation based on the nominal trajectory as a last line of defense against mid-air collision that minimizes the nuisance alarm [16]. However, ACAS II only offers protection against cooperative traffic with the appropriate equipage.

More recently, the advancement in machine learning and wider availability of the automatic dependent surveillance–broadcast (ADS-B) transponder led to the development of collision detection and resolution (CD&R) using the data-driven approach that predicts likely changes to trajectories of potential “intruder” and other traffic in the area [17,18]. The use of dynamic programming with historical traffic data by MIT Lincoln Lab’s uncorrelated encounter model would allow the CD&R function to recommend a resolution action with the least disruption to existing traffics within the airspace of operation. Further development of the encounter model to include probable mitigation actions by the pilots and air traffic controllers (ATCs) under correlated encounters were used to evaluate the new ACAS X algorithm [19,20]. The Bayesian network needed to support the ACAS X database requires a massive amount of track data from a wide range of aircraft types, which is not available for UTM. While works have been conducted to adapt the encounter model using data from hobbyist UAS tracks (the majority of which were non-cooperative) [21], those flight profiles differ greatly from the envisioned (but not from the existent) structured UTM network, where participants are cooperative.

While no consensus on the concept of operation for UTM has been reached at this time, recent works on UAS separation assurance follow two different ConOps: the free flight with detect and avoid (DAA) that requires some level of autonomy [22–25], and structured flights on established routes with separation standards [26–28]. The latter typically utilizes a Reich-inspired model for separation evaluation with a probabilistic distribution function taken from civil aviation. A common distribution function used for the Reich collision risk model is the double–double–exponential (DDE) distribution, which is described by a data-driven exponential distribution for the “core” zone and a more conservative “tail” zone often scaled to match the existing separation minima combined with a blending constant. Analysis has shown that collision risk is strongly dependent on the values chosen for the blending constant and the shaping parameter for the “tail” zone, especially in cases where the “core” distribution is significantly reduced with the availability of the global navigation satellite system (GNSS) [29].

More recently, the Reich collision risk model was further modified to account for the improvements in surveillance technologies and reduction in communication time with the aim of reducing the separation minima [30,31]. These changes to the time scale used in collision risk modeling are closer to those of tactical separation assurance (in the order of tens of seconds) than the traditional strategic separation assurance (in the order of half hours or longer). With the higher density of communication infrastructures in urban airspace, these timings might see further reductions in urban UTM, as discussed in Section 3.3.

3. Simulation and Model Setup

The implementation of the Reich collision risk model from ICAO Doc 9689 [12] was modified for Monte Carlo simulation with multirotor flight mechanics. The basic formulation and concept (see Figure 1) for the Reich collision risk model remains unchanged along with the assumption that mid-air collision would always results in fatality. The generalized Reich model utilizes DDE derived from the historical traffic data λ_{core} and additional allowance for pilot blunder λ_{tail} , neither of which is available for UTM traffic. While other studies have suggested that UTM traffic would follow a similar positional distribution to a fixed wing when operating along a fixed route, those distributions and mixing model were data driven in operational environments very different from urban UTM. Instead, the distribution of the UAS position at various look-ahead times is obtained using physics-based Monte Carlo modeling [32]. The distribution is then checked for

overlap with the collision volume of the other aircraft in the encounter pair to obtain the collision probability.

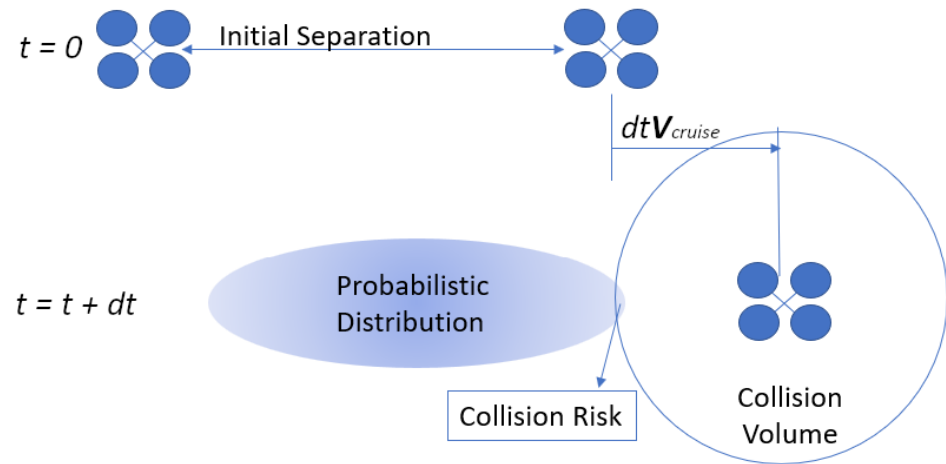


Figure 1. Concept for evaluation of separation recommendations.

The flight track for each of the Monte Carlo samples was generated with randomized velocity, heading angle, and elevation angle at each time step. These randomized variables were initially generated following the normal distribution between the range described in Equation (1):

$$\begin{cases} |V| \sim \mathcal{N}(|V_{target}|, 0.04|V_{max}|), |V_{max}| = 20 \text{ m/s} \\ \theta \sim \mathcal{N}(\theta_{target}, 0.0004\theta_{max}), \theta_{max} = 180^\circ \\ \phi \sim \mathcal{N}(\phi_{target}, 0.0025\phi_{max}), \phi_{max} = 90^\circ \end{cases} \quad (1)$$

where $|V|$ is the velocity magnitude, θ is the heading angle, and ϕ is the elevation angle. The variances for the heading and elevation angles were based on the performance parameters for the inertial measurement unit (IMU) without external (e.g., GNSS) corrections. The target heading and elevation angles (θ_{target} and ϕ_{target} , respectively) could be pointing towards the travel direction from a previous time step [32] towards the waypoint for the guidance segment [33], or towards a virtual waypoint within the guidance segment to enforce a set cruise speed (similar to the way PX4 flight controller handles position set points using the FlightTaskAuto module). Table 1 listed the symbols used in the following section.

Table 1. Table of Symbols for Section 3.

Symbol	Meaning
θ	heading angle
ϕ	elevation angle
T	thrust vector
K_d	empirical drag constant
\hat{u}	UAS attitude unit vector
ω	tilt angle
\hat{v}	UAS velocity unit vector

3.1. Emulation of PID

The typical feedback-control loop for a multirotor consists of two sequential segments: the position control segment and the attitude control segment. Each of these segments further consists of two cascading PID loops, one for the rate difference and one for the value difference. In the case of the PX4 controller (valid as of PX4 version 1.13.2.), the cascading loop takes the form of P-PID for the rate and value, i.e., for the attitude controller,

a proportional controller was applied on the angular velocity difference and a full position-integral-differential controller was applied on the angular value difference [34]. These controllers typically operate at a frequency of 250 Hz, which could place considerable computational burden on the hardware used for simulations, especially when dealing with a large number of Monte Carlo sample/agents. As such, the path-keeping function of the flight controller was emulated at $dt = 0.1$ s (10 Hz) instead by assuming that the attitude of the vehicle would always match the prescribed attitude pointing towards the virtual waypoint set by the flight task manager [35]. These assumptions were reinforced with the vehicle dynamics model described in Section 3.2 to ensure that only physical motions could be prescribed.

To emulate the track-keeping algorithm of the flight task manager, the virtual waypoint is set to a distance of $|V_{cruise}| \cdot dt$ on the assigned track from the last reported position of the UAS. This setup would allow $|V_{target}| > |V_{cruise}|$ for the vehicle position with a sufficiently large cross track or vertical deviation from the desired track, allowing the vehicle to catch up on the targeted trajectory. Note that the baseline $|V_{cruise}|$ was set to 10 m/s, with sensitivity analysis on separation evaluation results performed for $|V_{cruise}| = [8, 10, 12, 14, 16, 18]$ m/s. $|V_{cruise}| = 20$ m/s was not tested, as cruising at the maximum horizontal speed limit would pose a penalty on the maneuverability.

3.2. Dynamic Modeling of Monte Carlo Samples

As action within each time step of each Monte Carlo samples would need to remain physical and realistic, the “valid” range of motions must pass through two checks. The first is with the valid range of values and the second is with the kinematic modeling. Since the heading and elevation angles follow spherical coordinates, the randomized heading and elevation angles were further truncated to $[-180^\circ, 180^\circ]$ and $[-90^\circ, 90^\circ]$, respectively, to approximate circular normal distribution in both directions; the truncation limits were rarely enforced with the given variance. As the flight controller allows angular velocity of up to 2π rad/s, no additional limits were placed on the valid heading and elevation angle range. Similarly, all velocity magnitude assignments must first conform to the electronic speed limits of the flight controller (see Table 2). The second check for physically achievable values would be performed by truncating the achievable velocities distribution based on the kinematic equation (Equation (2)):

$$a = \frac{dV}{dt} = \frac{(T - mg - K_d V^2)}{m} \quad (2)$$

with $|T| = 0$ N and empirically estimated drag ($K_d V^2$) from the initial attitude for the lower limit. In Equation (2), a is the acceleration vector, T is the thrust vector, K_d is the empirical drag constant, and V is the velocity vector. As an example, the upper limit for the velocity magnitude is set to the maximum achievable velocity with full thrust input $|T| = |T_{max}|$ or the electronic speed limits in Table 2, whichever is lower. The selection of DJI Mavic 2 for the simulation is due to the availability of the aircraft for the physical measurement and of the flight trajectory data.

Table 2. Performance specifications of DJI Mavic 2.

Variable	Value
UAS Mass (m) [36]	0.9 kg
Maximum Horizontal Speed (S-mode) [36]	20 m/s
Maximum Tilt Angle (S-mode) [36]	35 degree
Maximum Horizontal Speed (P-mode) [37]	14 m/s
Maximum Tilt Angle (P-mode) [36]	25 degree
Maximum Ascend Speed [36]	4 m/s
Maximum Descend Speed [36]	3 m/s

The empirical drag constant K_d varies with multirotor attitude and is related to the axial (K_{da}) and radial (K_{dr}) drag constants via Equation (3):

$$K_d V^2 = K_{da} (V \sin \omega)^2 + K_{dr} (V \cos \omega)^2. \quad (3)$$

The derivation of the axial and radial drag constants for DJI Mavic 2 were presented in a previous paper [32]. With the initial thrust and drag forces established, the next step is to determine the thrust vector for the current time step to achieve the assigned target velocity vector from Equation (1) as bracketed by UAS kinematics. Assuming that attitude change occurs instantaneously at the beginning of each time step, the thrust vector of the multirotor would be aligned with its attitude vector (with unit vector \hat{u}) instead of the assigned velocity vector (with unit vector $\hat{v} = \mathbf{V}/|\mathbf{V}|$). The attitude unit vector could also be described using the attitude tile angles relative to the global reference frame, with ω_1 as the angle about the x-axis and ω_2 about the y-axis, with y-axis being the direction of travel. \hat{u} could then be written as

$$\hat{u} = \begin{bmatrix} \cos \omega_1 \sin \omega_2 \\ -\sin \omega_1 \\ \cos \omega_1 \cos \omega_2 \end{bmatrix}. \quad (4)$$

Further assumption that the velocity change occurs instantaneously at the beginning of each time step means that the thrust magnitude for the current time step would need to be in balance with the gravitation force and the drag force. The drag force in this case would be along the direction of $-\hat{v}$, which could be expressed in the pitch (ϕ) and yaw (θ) angles that are randomly assigned at the beginning of the time step. Thus, the unit vector for the velocity could be written as

$$\hat{v} = \begin{bmatrix} \sin \theta \cos \phi \\ \cos \theta \cos \phi \\ \sin \phi \end{bmatrix} \quad (5)$$

and allows the drag vector to be written as

$$\mathbf{D} = -\hat{v} [K_{da} (\mathbf{V} \cdot \hat{u})^2 + K_{dr} (\mathbf{V} \cdot (\hat{v} - (\hat{v} \cdot \hat{u}))^2)] \quad (6)$$

which could be plugged back into Equation (2) with the assumption of $\mathbf{a} = 0$ to solve for $|\mathbf{T}|$ by iteratively changing ω , and thus \hat{u} , until $\mathbf{T} \cdot \hat{u} = 0$ using the bisection method. The values for ω were limited to

$$0 < \cos \omega_1 \cos \omega_2 < \cos 40^\circ \quad (7)$$

which were also used as the initial search interval. The resulting thrust vector is used to calculate the limits for the velocity vector assignment for the subsequent time step. The position of the vehicle at the end of the time step is calculated using the assigned velocity multiplied by the time step size. This is also where a randomized domain wide wind velocity could be injected into position updates, which is not considered in the current study. The statistics on the output from the flight track generation with 10^7 samples is presented in Table 3. Note that a slight growth in position error over time was observed from the simulation results in all three directions when such growth was not observed in the experimental flight technical error (FTE) data from lower cruise speed (the experimental data were collected with a cruise speed of 7 m/s). The growth in the position distribution (as represented by σ) remained small, going from 1.22 m to 3.42 m in the longitudinal direction and 0.63 m to 1.29 m in the lateral direction over a travel distance of over 200 m. This could be a consequence of the larger time step sizes used ($dt = 0.1$ s) in the simulation that would allow the aircraft to travel a larger distance before velocity corrections were made. Note that the longitudinal distribution at $t = 20$ s has an excess kurtosis of 1.33, making σ unsuitable for the distribution prediction.

Table 3. Statistics on the 10^7 output from Monte Carlo simulation with track correction enabled.

Longitudinal (Along-Track)				
Time (s)	Mean (m)	Median (m)	95% CI (m)	σ (m)
5	50.35	50.35	49.45/198.19	0.46
10	100.70	100.70	99.42/101.98	0.65
15	151.02	151.03	149.39/152.61	0.83
20	200.30	200.34	198.19/202.19	1.04
Lateral (Cross-Track)				
Time (s)	Mean (10^{-3} m)	Median (10^{-3} m)	95% CI (m)	σ (m)
5	−2.1	−2.7	−0.88/0.87	0.45
10	−2.5	−3.9	−1.24/1.23	0.63
15	−6.0	−5.3	−1.53/1.51	0.78
20	−8.8	−8.8	−1.78/1.75	0.89
Vertical				
Time (s)	Mean (10^{-2} m)	Median (10^{-2} m)	95% CI (m)	σ (m)
5	0.49	0.47	−0.98/0.98	0.50
10	0.68	0.67	−1.23/1.24	0.63
15	1.15	1.16	−1.35/1.36	0.69
20	1.46	1.26	−1.42/1.43	0.72

3.3. Collision Assessment with Varying Encounter Geometries

For collision assessment, positional distributions at different time steps were taken directly from the Monte Carlo simulations and placed into the collision assessment domain. The collision volume was inserted into the same domain each time step at the prescribed position. For example, in the same-track evaluation, the collision volume is inserted at a horizontal distance equal to the initial separation from the “follower” multirotor at $t = 0$ s and travel in the track direction for a further $0.1 \times |V_{cruise}|$ at $t = 0.1$ s. A count of overlap between the sample distribution and the collision volume using the `inpolygon` function would give the collision probability inferred by the sample size.

A stadium-cylinder-shaped collision volume was used in the collision assessment, with the collision volume being attached to the “leader” aircraft. The top-down profile of the stadium consists of semi-circles with radii equal to the sum of the navigation system error (NSE) from both aircraft and straight segments of length $|V_{horizontal}| \cdot dt$. This assumes that NSE is the same along both horizontal directions, which might not be true in highly built-up areas, where directional bias might exist. For very small time step sizes, the collision volume would approach the shape of a right circular cylinder. The sizing for the collision volume was set in previous studies with $NSE_{horizontal} = 1$ m and $NSE_{vertical} = 22.5$ m, with the latter adopted from the ACAS II vertical miss distance with a barometric altimeter. A sensitivity analysis of the separation evaluation outputs was performed for $NSE_{horizontal} = [1, 2, 5, 30]$ m and $NSE_{vertical} = [1, 2, 5, 22.5]$ m.

In this study, a total of 10^7 samples were used in the simulation. With the assumption of one mid-air-collision (MAC) event per flight hour, this would infer a collision probability of less than 10^{-7} MAC/flight hour (MAC threshold proposed [8]) if no collision was detected over the length of the simulation. The assumption that any collision would result in fatality is used to convert the collision probability to the collision risk of 10^{-7} fatal event/flight hour.

The baseline simulation length was set to 20 s, which consists of the maximum update interval for ADS-B before the position is considered no longer valid, the pilot and controller reaction time, and some “communication” time to round off the simulation time to the nearest 10 seconds. A breakdown of the time components and the sources (if applicable) is shown in Table 4. This is meant to represent the maximum time gap it would take for a

separation breach to be determined and communicated; the escape maneuver time was not considered currently due to the assumption that the immediate speed reduction could be taken given the small multirotor flight dynamics. Sensitivity analysis of the separation evaluation outputs was performed for the simulation length of $t_{total} = [20, 30, 40]$ s.

Table 4. Breakdown of collision simulation time budgeting for performance-based separation evaluation.

Component	Time (s)	Remarks
ADS-B Update Interval [38]	3	ADS-B update interval before considered as signal lost
Pilot Reaction [39]	5.7	Pilot reaction to controller commends and enact corrective actions
ATC Reaction [39]	7.6	ATC reaction to server warning and relay it to pilot
Communication Time	2.7	Arbitrary additional time to round off to nearest 10
Total	20	-

The collision geometries were condensed to the same track, parallel tracks, and vertically stacked tracks to emulate the basic encounter scenarios under a structured UTM airway system. The leader and follower aircraft were placed at an initial separation distance bracketing the guessed separation recommendations based on the assigned NSE and experimentally derived FTE. For parallel and vertical-stacked tracks, the leader and follower aircraft were initialized with the same along-track position (see Figure 2). The assigned tracks were assumed to be straight and without altitude change. The more complex encounter geometries involving crossing tracks of various angles were not considered.

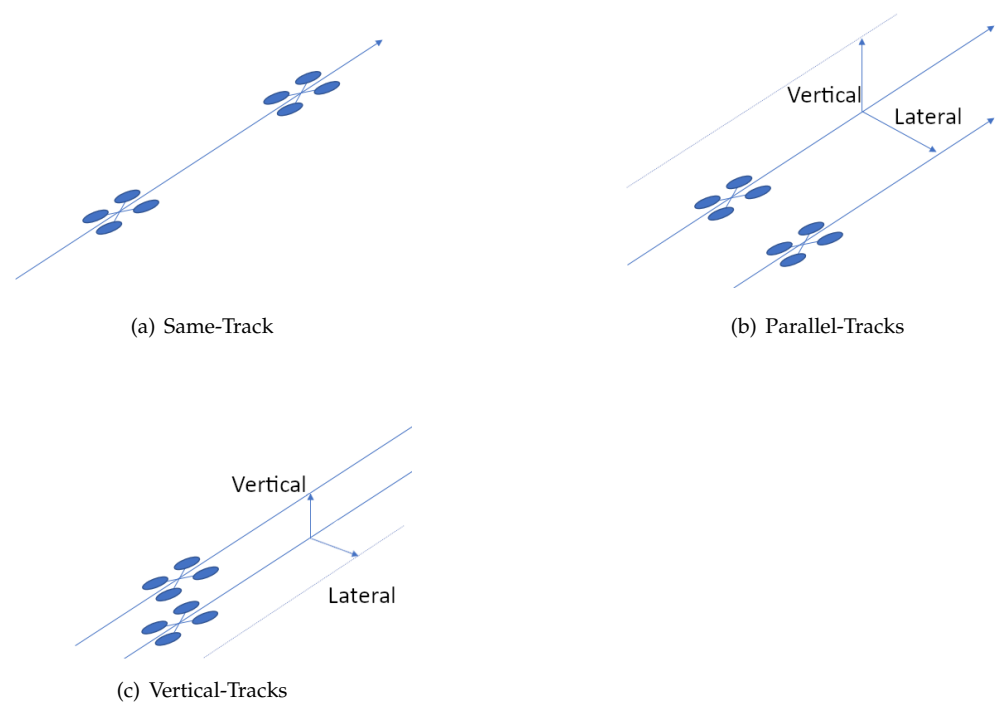


Figure 2. Schematics showing the initial positions and assigned tracks for the three encounter geometries tested.

4. Results and Discussion

The separation evaluation results using the modified Reich collision risk model with distribution estimated with Monte Carlo UAS samples are presented below. The baseline encounter case utilizes the following parameters: $t_{total} = 20$ s, $V_{cruise} = 10$ m/s, $NSE_{horizontal} = 1$ m, and $NSE_{vertical} = 22.5$ m. Parametric studies were performed for the same-track, parallel-track, and vertically stacked-track encounter geometries by varying the look-ahead time ($T_{total} = [20, 30, 40]$ s, Table 5), the target cruise speed ($|V_{cruise}| = [8, 10, 12, 14, 16, 18]$ m/s, Table 6), and the estimated navigation error ($NSE_{horizontal} = [1, 2, 5, 30]$ m and $NSE_{vertical} = [1, 2, 5, 22.5]$ m, Table 7) for the airspace. A visualization of the same-track and parallel-track setup with reduced sample size is shown in Figure 3. Note that the increase in look-ahead time would also increase the distance traveled by both aircraft over the risk-assessment period, possibly leading to wider position uncertainties, even if the trajectory deviation over the travel distance remains the same.

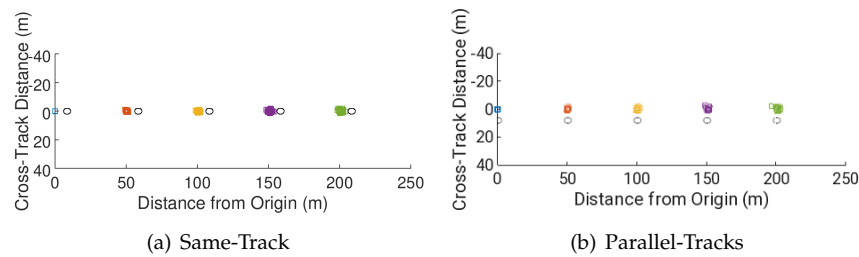


Figure 3. Sample outputs visualized at 5 s intervals with 20 Monte Carlo samples in (a) same track and (b) parallel track encounter geometries.

Table 5. Sensitivity analysis of separation recommendations with varying look-ahead time (t_{total}).

Same Track			
t_{total} (s)	V_{cruise} (m/s)	Equivalent NSE (m)	Sep. Recomm. (m)
20	10	1	8.2
30	10	1	9.7
40	10	1	11.7
Parallel Tracks			
t_{total} (s)	V_{cruise} (m/s)	Equivalent NSE (m)	Sep. Recomm. (m)
20	10	1	6.0
30	10	1	6.1
40	10	1	6.5
Vertical Tracks			
t_{total} (s)	V_{cruise} (m/s)	Equivalent NSE (m)	Sep. Recomm. (m)
20	10	22.5	26.6
30	10	22.5	27.6
40	10	22.5	28.4

The parametric study showed some impact of the look-ahead time on the same-track separation recommendation, which is consistent with the increase in the spread of sample distribution over time (as seen in Table 3). However, the results suggest that the increase in separation recommendation is not linear with time, nor does it follow the same trend as the increase in σ over time, making it impossible to predict the separation recommendation

for a longer look-ahead time using simple extrapolation. Furthermore, the longitudinal distribution of the multirotor positions appears to be tied to the trajectory planning methods used to generate interim position set-point along the assigned track, making it suitable only for the current mission control algorithm. Alternatively, an assumption could be made that future revision of the mission control algorithm would be made to enable trajectory-based operations, thus making the longitudinal position distribution time independent, similar to that of the lateral distribution. This could mean that the look-ahead time might not be as critical of an issue for separation prediction with the future generation of the mission controller.

On the other hand, the effect of the look-ahead time on the parallel and vertically stacked tracks is minimal, as the cross-track and altitude error were more tightly managed by the track-keeping and altitude-keeping algorithm. The results suggests that from an air-corridor-planning perspective, the separation evaluation for parallel/vertically stacked could be performed without involving a long look-ahead time. Note that the current setup assumes an occupancy ($E_{y/z}$ from ICAO 9689) of one encounter per hour; for a less crowded airspace, this number could be significantly lower than 1, which would reduce the lateral/vertical separation recommendation further.

Table 6. Summary of separation evaluation results for CNS-based separation with varying V_{cruise} .

Same Track		
V_{cruise} (m/s)	Equivalent NSE (m)	Sep. Recomm. (m)
8	1	8.1
10	1	8.2
12	1	7.8
14	1	7.2
16	1	6.1
18	1	5.2
Parallel Tracks		
V_{cruise} (m/s)	Equivalent NSE (m)	Sep. Recomm. (m)
8	1	5.3
10	1	6.0
12	1	6.3
14	1	6.8
16	1	6.4
18	1	6.3
Vertical Tracks		
V_{cruise} (m/s)	Equivalent NSE (m)	Sep. Recomm. (m)
8	22.5	25.9
10	22.5	26.6
12	22.5	27.2
14	22.5	28.2
16	22.5	28.9
18	22.5	29.9

Results from the parametric studies on cruise velocity are in line with the expectation that the position distribution would reduce as the cruise velocity approaches the electronic speed limit. This expectation stems from the reduced velocity truncation range near the flight controller enforced speed limits. Additionally, since the virtual waypoint was computed to return the aircraft to the assigned track following the target cruise speed, the residual thrust after correcting for heading and elevation deviation might not be sufficient to meet the target cruise speed set along the longitudinal direction. The priority of the attitude correction over the horizontal speed target would result in lower corrections for the lateral and vertical deviations as the target cruise speed approaches the speed limits. Thus, a reduced lateral and vertical distribution range was observed with less impact on the separation recommendations for parallel and vertical tracks.

It should be noted that the electronic speed limits exist to ensure the flight stability of the multirotor, as studies have shown that stable air speed (or cross-wind speed when hovering) could be drastically reduced when subjected to even a modest level of turbulence intensity [40]. It should also be noted that the implementation of a virtual waypoint in this study is ground-speed based, making it unsuitable for collision analysis in windy conditions without additional airspeed limits to address the stability concerns.

Table 7. Summary of separation evaluation results for CNS-based separation with varying NSE.

Same Track		
V_{cruise} (m/s)	Equivalent NSE (m)	Sep. Recomm. (m)
10	1	8.2
10	2	10
10	5	16.1
10	30	66.5
Parallel Tracks		
V_{cruise} (m/s)	Equivalent NSE (m)	Sep. Recomm. (m)
10	1	6.0
10	2	7.8
10	5	14.1
10	30	65
Vertical Tracks		
V_{cruise} (m/s)	Equivalent NSE (m)	Sep. Recomm. (m)
10	1	5.1
10	2	6.0
10	5	6.8
10	22.5	26.6

The final parameter studied is the effect of navigation uncertainties, which are directly tied to the radius and height of the collision volume, on separation recommendations. The resulting separation shows a near linear relationship between the increase in NSE and the resulting separation recommendations, e.g., $(2 \times 1 + 8.2) - 10 = 0.2$ for $NSE = 2$ ($2 \times NSE + 8.2$ (separation recommendation at $NSE = 1$) while $(2 \times 29 + 8.2) - 66.5 = -0.3$. The slightly smaller difference at larger NSE might be due to the flatter curvature of the collision volume with a larger radius, but this impact does not appear to be significant. Overall, the effect of varying NSE on the separation evaluation appears to be linear and is consistent with the expected trend. Note that the current model is unable to simulate the

change in the size and shape of the NSE bound as the multirotor moves through the urban environment, where the navigation performance might differ from one block to the next.

5. Conclusions

Separation evaluations were performed for structured UTM using a modified Reich collision risk model that uses Monte Carlo samples to generate follower aircraft tracks and position distributions. A virtual waypoint flight management algorithm was used to emulate the PID controller's enforcement of the target cruise speed and track keeping. Parametric studies were performed for an identical quadrotor encounter pair of $M \sim 1.2$ kg on the look-ahead time, target cruise speed, and navigation uncertainties for traffic encounters in same-track, parallel-track, and vertically stacked-track geometries. The collision-risk threshold for determining the separation recommendations was set to $TLOS \leq 10^{-7}$ collision/flight hours.

The simulation results indicated that while along-track separation varies with the look-ahead time due to the design of the mission control algorithm, the length of the look-ahead time has only a minor influence on the parallel-track and vertical-track separation recommendations. On the other hand, the changes to the target cruise speed have a much smaller effect on the separation recommendations, showing only a minor reduction in separation as the target cruise speed approaches the electronic speed limit of the aircraft. Finally, navigation uncertainties were shown to have a significant effect on the separation recommendations, mostly due to the NSE directly affecting the collision volume sizing. Overall, the results showed that the Monte Carlo approach to separation evaluation for UTM under the Reich framework is still needed with the current generation of UAS flight controllers, especially in the longitudinal direction. The results also highlighted the need for better understanding of NSE in urban environments, where the degradation of navigation performance is expected.

Some of the major limitations of the current approach include the simplifications made to the flight controller behavior and the reduced update frequency, both made to conserve computational resources. Another limitation of the Reich-based approach is the lack of consideration for response by ATC and the remote pilot; this is more difficult to model due to the lack of understanding towards the ATC–remote pilot interaction under UTM settings. Finally, since the target level of safety in UTM is driven by ground fatality instead of passenger fatality, a discussion must be made in the future on the appropriateness of using the operation-based TLOS value instead of the cumulative societal-risk targets.

Author Contributions: Conceptualization, C.-H.J.W. and C.D.; methodology, C.-H.J.W.; software, C.-H.J.W.; data curation, C.D.; writing—original draft preparation, C.-H.J.W.; writing—review and editing, C.-H.J.W. and K.H.L.; funding acquisition, K.H.L. All authors have read and agreed to the published version of the manuscript.

Funding: This research received no external funding.

Data Availability Statement: Data sharing not applicable.

Acknowledgments: This project is supported by the National Research Foundation, Singapore, and the Civil Aviation Authority of Singapore, under the Aviation Transformation Program on Unmanned Aircraft Systems (UAS) in the topic of Separation Minima. The support from Air Traffic Management Research Institute (ATMRI) and the School of Mechanical and Aerospace Engineering (MAE), Nanyang Technological University (NTU) is also appreciated. Any opinions, findings and conclusions or recommendations expressed in this material are those of the authors and do not reflect the views of National Research Foundation, Singapore and the Civil Aviation Authority of Singapore. The simulation was made possible by the computational resource allocated by the National Supercomputing Center (NSCC) under project account 12002591.

Conflicts of Interest: The authors declare no conflict of interest.

References

1. Vrijling, J.; van Hengel, W.; Houben, R. A framework for risk evaluation. *J. Hazard. Mater.* **1995**, *43*, 245–261. [[CrossRef](#)]
2. Vrijling, J.H.K.; van Gelder, P.H.A.J.M.; Goossens, L.H.J.; Voortman, H.G.; Pandey, M.D. A framework for risk criteria for critical infrastructures: Fundamentals and case studies in the Netherlands. *J. Risk Res.* **2004**, *7*, 569–579. [[CrossRef](#)]
3. Liu, P.; Yang, R.; Xu, Z. How Safe Is Safe Enough for Self-Driving Vehicles? *Risk Anal.* **2018**, *39*, 315–325. [[CrossRef](#)] [[PubMed](#)]
4. Fischhoff, B.; Slovic, P.; Lichtenstein, S.; Read, S.; Combs, B. How safe is safe enough? A psychometric study of attitudes towards technological risks and benefits. *Policy Sci.* **1978**, *9*, 127–152. [[CrossRef](#)]
5. Kaneko, F.; Arima, T.; Yoshida, K.; Yzui, T. On a Novel Method for Approximation of FN Diagram and Setting ALARP Borders. *J. Mar. Sci. Technol.* **2015**, *20*, 13–40. [[CrossRef](#)]
6. Garrett-Glaser, B. Industry and regulators look to each other for progress, harmonization on eVTOL certification requirements. *Vertical* **2020**. Available online: <https://verticalmag.com/features/industry-regulators-look-each-other-progress-evtol-certification-requirements/> (accessed on 7 May 2023).
7. Pasma, H.; Vrijling, J. Social risk assessment of large technical systems. *Hum. Factors Ergon. Manuf. Serv. Ind.* **2003**, *13*, 305–316. [[CrossRef](#)]
8. Vila Carbó, J.A.; Iocchi, L. *Algorithm for Analysing the Collision Risk*; Technical Report D4.1; SESAR Joint Undertaking: Brussels, Belgium, 2021.
9. Brooker, P. Air Traffic Control Separation Minima: Part 1—The Current Status. *J. Navig.* **2011**, *64*, 449–465. [[CrossRef](#)]
10. Reich, P.G. Analysis of Long-Range Air Traffic Systems: Separation Standards III. *J. Navig.* **1966**, *19*, 331–347. [[CrossRef](#)]
11. Machol, R.E. Thirty Years of Modeling Midair Collisions. *Interface* **1995**, *25*, 151–172. [[CrossRef](#)]
12. ICAO. *Manual on Airspace Planning Methodology for the Determination of Separation Minima*, 1st ed.; International Civil Aviation Organization: Montreal, QC, Canada, 1998.
13. Civil, J.; Daly, H. The Longitudinal Reich Collision Risk Model. In Proceedings of the Separation and Airspace Safety Panel (SASP) Meeting of the Working Group of the Whole, Montreal, QC, Canada, 14–25 May 2012; Number SASP-WG/WHL/20 IP/10.
14. Krozel, J.; Peters, M.E.; Hunter, G. *Conflict Detection and Resolution for Future Air Transport Management*; Technical Report NASA-CR-97-295944; NASA Ames Research Center: Moffett Field, CA, USA, 1997.
15. Kuchar, J.K.; Yang, L.C. A Review of Conflict Detection and Resolution Modeling Methods. *IEEE Trans. Intell. Transp. Syst.* **2000**, *1*, 179–189. [[CrossRef](#)]
16. EUROCONTROL. (Ed.) *ACAS Guide: Airborne Collision Avoidance Systems*, 4.1st ed.; European Organisation for the Safety of Air Navigation: Brussels, Belgium, 2022.
17. Weinert, A.J.; Harkleroad, E.P.; Griffith, J.D.; Edwards, M.W.; Kochenderfer, M.J. *Uncorrelated Encounter Model of the National Airspace Version 2.0*; Number ATC-404; Lincoln Laboratory, Massachusetts Institute of Technology: Lexington, MA, USA, 2012.
18. Underhill, N.; Weinert, A. Applicability and Surrogacy of Uncorrelated Airspace Encounter Models at Low Altitudes. *J. Air Transp.* **2021**, *29*, 137–141. [[CrossRef](#)]
19. Kochenderfer, M.J.; Holland, J.E.; Chryssanthacopoulos, J.P. Next-Generation Airborne Collision Avoidance System. *Linc. Lab. J.* **2012**, *19*, 17–33.
20. Owen, M.P.; Panken, A.; Moss, R.; Alvarez, L.; Leeper, C. ACAS Xu: Integrated Collision Avoidance and Detect and Avoid Capability for UAS. In Proceedings of the 2019 IEEE/AIAA 38th Digital Avionics Systems Conference (DASC), San Diego, CA, USA, 8–12 September 2019; pp. 1–10. [[CrossRef](#)]
21. Muller, E.; Kochenderfer, M.J. Simulation Comparison of Collision Avoidance Algorithms for Small Multi-Rotor Aircraft. In Proceedings of the AIAA Modeling and Simulation Technologies Conference, San Diego, CA, USA, 4–8 January 2016. [[CrossRef](#)]
22. Lee, S.M.; Park, C.; Johnson, M.A.; Mueller, E.R. Investigating Effects of “Well Clear” Definitions on UAS Sense-and-Avoid Operations in Enroute and Transition Airspace. In Proceedings of the 2013 Aviation Technology, Integration, and Operations Conference, Los Angeles, CA, USA, 12–14 August 2013. [[CrossRef](#)]
23. Duffield, M.O.; McLain, T.W. A Well Clear Recommendation for Small UAS in High-Density, ADS-B-Enabled Airspace. In Proceedings of the AIAA SciTech Forum, Grapevine, TX, USA, 9–13 January 2017. [[CrossRef](#)]
24. Weinert, A.; Campbell, S.; Vela, A.; Schuldt, D.; Kurucar, J. Well-Clear Recommendation for Small Unmanned Aircraft Systems Based on Unmitigated Collision Risk. *J. Air Transp.* **2018**, *26*, 113–122. [[CrossRef](#)]
25. Khan, A.; Jiménez, C.A.C.; Pablo, M.P.; Ivaki, N.; Tejedor, J.V.B.; Madeira, H. Assessment of the Impact of U-space Faulty Conditions on Drones Conflict Rate. In Proceedings of the Computer Safety, Reliability, and Security, Munich, Germany, 6–9 September 2022; Springer International Publishing: Berlin/Heidelberg, Germany, 2022; pp. 237–251.
26. McFadyen, A. Probabilistic Determination of Maximum Safe Altitude for Unmanned Traffic Management. In Proceedings of the IEEE/AIAA 38th Digital Avionics System Conference (DASC), San Diego, CA, USA, 8–12 September 2019. [[CrossRef](#)]
27. Kallinen, V.; McFadyen, A. Collision Risk Model and Analysis for Lateral Separation to Support Unmanned Traffic Management. *Risk Anal.* **2022**, *42*, 854–881. [[CrossRef](#)] [[PubMed](#)]
28. Kim, Y.; Bae, J. Risk-Based UAV Corridor Capacity Analysis above a Populated Area. *Drones* **2022**, *6*, 221. [[CrossRef](#)]
29. Nagoka, S.; Amai, O. *An Analysis on the Effect of Lateral Offsets on the Lateral Collision Risk of the NOPAC Routes*; Technical Report APANPIRG 13-IP11; International Civil Aviation Organization: Montreal, QC, Canada, 2003.

30. Louis, L.S. *WP4 Final Report and Annex with Refined DOD Examples*; Technical Report D4.4; European 6th RTD Framework Programme; European Commission: Brussels, Belgium, 2010.
31. Tošić, V.; Mirković, B. Investigating Untapped Capacity at Single-Runway Airports using Short Final Curved Approach, Dual Glide Slope, and Double Threshold. *Transp. Res. Rec.* **2020**, *2674*, 1136–1146. [[CrossRef](#)]
32. Wang, C.H.J.; Tan, S.K.; Low, K.H. Three-Dimensional (3D) Monte-Carlo Modeling for UAS Collision Risk Management in Restricted Airport Airspace. *Aerosp. Sci. Technol.* **2020**, *105*, 105964. [[CrossRef](#)]
33. Wang, C.H.J.; Ng, E.M.; Low, K.H. Investigation and Modeling of Flight Technical Error (FTE) Associated with UAS Operating with and without Pilot Guidance. *IEEE Trans. Veh. Technol.* **2021**, *70*, 12389–12401. [[CrossRef](#)]
34. Dronecode Project Inc. PixHawk 4 Firmware, 2023. v1.13. Available online: <https://www.github.com/PX4/PX4-Autopilot> (accessed on 1 January 2023).
35. Wang, C.H.J.; Deng, C.; Low, K.H. Same-Track UAS Separation Requirement Evaluation with Monte-Carlo based Collision Risk Modeling. In Proceedings of the AIAA SciTech Forum, Orlando, FL, USA, 8–12 January 2024. [[CrossRef](#)]
36. DJI Technology Co., Ltd. *Mavic 2 Zoom User Manual*, 2.2nd ed.; SZ DJI Technology Co., Ltd.: Shenzhen, China, 2020.
37. Mavic 2 Enterprise. Available online: <https://www.dji.com/mavic-2-enterprise/specs> (accessed on 1 April 2018).
38. *Automatic Dependent Surveillance-Broadcast (ADS-B) Flight Inspection*; Federal Aviation Administration: Washington, DC, USA, 2014.
39. Everdji, M.H.C.; Blom, H.A.P.; Bakker, G.J.; Zmarrou, H. Agent-Based Safety Risk Analysis of Time Based Operation in Future TMA. In Proceedings of the Third International Air Transport and Operations Symposium, Delft, The Netherlands, June 2012; pp. 443–457. [[CrossRef](#)]
40. Barber, H.; Wall, A.; Tabachnick, I. *RPAS Operator Guidance and Safety Assurance Tools for the Urban Environment: Phase II*; Technical Report LTR-AL-2022-0010; National Research Council of Canada, Aerospace Research Centre, Aerodynamics Laboratory: Ottawa, ON, Canada, 2022. [[CrossRef](#)]

Disclaimer/Publisher’s Note: The statements, opinions and data contained in all publications are solely those of the individual author(s) and contributor(s) and not of MDPI and/or the editor(s). MDPI and/or the editor(s) disclaim responsibility for any injury to people or property resulting from any ideas, methods, instructions or products referred to in the content.